Aalborg Universitet

LTP Modeling of Single-Phase T/4 Delay-Based PLLs

Golestan, Saeed; Guerrero, Josep M.; Vasquez, Juan C.

LTP Modeling of Single-phase $T/4$ Delay-Based PLLs

Saeed Golestan, *Senior Member, IEEE, Member, IEEE,* Josep M. Guerrero, *Fellow, IEEE,*
and Juan C. Vasquez, *Senior Member, IEEE*

Abstract—**A large number of single-phase phase-locked loops (PLLs) require generating a $90°$ phase-shifted version of their single-phase input signal. Among the wide variety of options, using a quarter-cycle transfer delay is particularly popular. In recent years, several single-phase transfer delay-based PLLs (TD-PLLs) have been proposed in the literature. The major difference between different TD-PLLs lies in the way they have adapted to frequency changes. Regardless of this structural difference, a common trend in investigating TD-PLLs is obtaining a linear time-invariant (LTI) model and analyzing it. Obtaining such a model, however, is often based on neglecting the input signal amplitude variations and double-frequency oscillations in the transient behavior of TD-PLLs, which results in some inaccuracies. To deal with this problem, the linear time-periodic (LTP) modeling of TD-PLLs is presented in this letter. It is demonstrated that the LTP model does not have the limitations of the LTI one and can provide much higher accuracy, but at the cost of a higher model complexity.**

Index Terms—**Linear time-invariant (LTI), linear time-periodic (LTP), modeling, orthogonal signal, phase-locked loop (PLL), single-phase systems, synchronization, transfer delay.**

I. INTRODUCTION

THE majority of single-phase PLLs try to mimic a three-phase synchronous reference frame PLL (SRF-PLL) structure [1], [2]. To this end, the single-phase input signal (with or without a pre-filtering) is considered as the α-axis input of the SRF-PLL, and a fictitious quadrature signal is generated and used as the β-axis input. Such a fictitious signal can be generated using different filters/algorithms/circuits, such as the second-order generalized integrator [3], all-pass filter [4], inverse Park Transform [5], Hilbert transform [6], Kalman filter [7], recursive discrete Fourier transform [8], and quarter-cycle transfer delay [9]–[12]. Here, the focus is on using the quarter cycle transfer delay, which is a simple and popular approach. The block diagram representation of a basic transfer delay-based PLL (TD-PLL) can be seen in Fig. 1.

The basic TD-PLL uses a fixed-length quarter cycle delay, which means the phase difference between its $\alpha\beta$-axis input signals may not be exactly $90°$ under off-nominal frequencies.
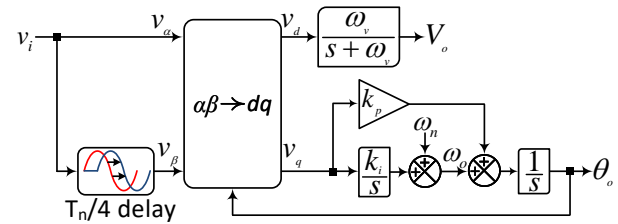
Fig. 1. Block diagram representation of the basic TD-PLL. v_i is the single-phase input. ω_n is the nominal angular frequency of v_i, and $T_n = \frac{2\pi}{\omega_n}$. ω_o, V_o, and θ_o are estimations of the fundamental angular frequency, amplitude, and phase angle of v_i, respectively. k_p, k_i, and ω_v are the control parameters.
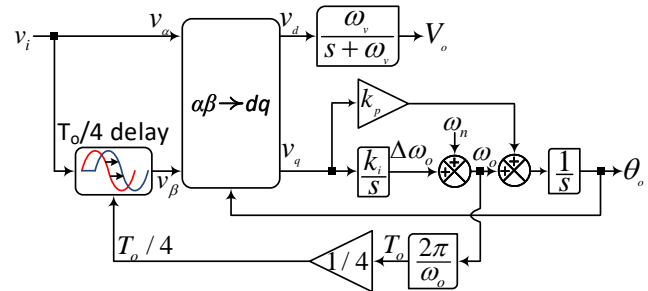
Fig. 2. Block diagram representation of the VLTD-PLL. T_o is an estimation of the fundamental period of the input signal. The delay length is variable.

This non-orthogonality causes offset and double-frequency oscillatory errors in the output of the basic TD-PLL under off-nominal frequencies [11]. To deal with this challenge, several approaches have been proposed in the literature. A possible method, as shown in Fig. 2, is adapting the length of the quarter cycle delay to frequency changes, which results in a variable-length TD-PLL (VLTD-PLL) [10], [12]. An alternative way is keeping the delay length constant and correcting the non-orthogonality between the $\alpha\beta$-axis input signals through a feedback loop, as shown in Fig. 3 [9]. This structure is called the adaptive TD-PLL (ATD-PLL). For a more detailed review of the basic TD-PLL and its advanced versions, refer to [1].

To facilitate the analysis of the basic TD-PLL and its advanced versions, which are all nonlinear feedback control systems, some linear time-invariant (LTI) models have been presented in the literature [9]–[11]. Obtaining these LTI models, however, is based on some assumptions, which may cause some inaccuracies. For instance, in developing the LTI models in [9]–[11], the input signal amplitude variations are neglected,

Fig. 3. Block diagram representation of the ATD-PLL.

which may not be accurate in grid applications. This letter aims to present more accurate linear models for single-phase $T/4$ delay-based PLLs. The modeling will be carried out in the linear time-periodic (LTP) framework. First, the ATD-PLL is considered as the case study, and its LTP modeling is presented. Based on the obtained LTP model and following an intuitive approach, the LTP models of the basic TD-PLL and VLTD-PLL are also obtained. It is discussed theoretically and demonstrated numerically that modeling in the LTP framework can provide higher accuracy in investigating TD-PLLs compared to the LTI framework.

II. ATD-PLL

A. LTP Modeling

The signal v'_β in Fig. 3 is equal to

$$v'_\beta(t) = \frac{v_\alpha(t - T_n/4) + v_\alpha(t)\overbrace{\sin(\Delta\omega_o T_n/4)}^{\approx(\Delta\omega_o T_n/4)}}{\underbrace{\cos(\Delta\omega_o T_n/4)}_{\approx 1}}. \quad (1)$$

By assuming the single-phase input signal $v_i = v_\alpha$ in Fig. 3 as (2), and defining its amplitude and phase angle as (3), (1) can be approximated by (4).

$$v_i(t) = v_\alpha(t) = V_i \cos(\theta_i) \quad (2)$$

$$\begin{aligned} V_i &= V_n + \Delta V_i \\ \theta_i &= \underbrace{\theta_n}_{\int \omega_n dt} + \Delta\theta_i \end{aligned} \quad (3)$$

$$\begin{aligned} v'_\beta(t) &\approx (V_n + \Delta V_i^d)\sin(\theta_n + \Delta\theta_i^d) \\ &+ \underbrace{(\Delta\omega_o T_n/4)(V_n + \Delta V_i)}_{\approx V_n(\Delta\omega_o T_n/4)}\cos(\theta_n + \Delta\theta_i) \end{aligned} \quad (4)$$

Notice that V_i and θ_i and, therefore, ΔV_i and $\Delta\theta_i$ in the above equations are functions of time. Notice also that $\Delta V_i^d(t) = \Delta V_i(t - T_n/4)$ and $\Delta\theta_i^d(t) = \Delta\theta_i(t - T_n/4)$.

Considering the above equations and the Park transformation in (5), in which $\theta_o = \theta_n + \Delta\theta_o$ is an estimation of θ_i, the signals v_d and v_q in Fig. 3 can be expressed as (6) and (7), respectively.

$$\begin{bmatrix} v_d(t) \\ v_q(t) \end{bmatrix} = \begin{bmatrix} \cos(\theta_o) & \sin(\theta_o) \\ -\sin(\theta_o) & \cos(\theta_o) \end{bmatrix} \begin{bmatrix} v_\alpha(t) \\ v'_\beta(t) \end{bmatrix} \quad (5)$$

Fig. 4. (a) LTP model of the ATD-PLL. (b) LTI model of the ATD-PLL [9]. Without loss of generality, $\theta_n = \omega_n t$ can be considered.

$$\begin{aligned} v_d(t) &\approx \frac{V_n + \Delta V_i}{2}\left[\cos(\Delta\theta_i - \Delta\theta_o) + \cos(2\theta_n + \Delta\theta_i + \Delta\theta_o)\right] \\ &+ \frac{V_n + \Delta V_i^d}{2}\left[\cos(\Delta\theta_i^d - \Delta\theta_o) - \cos(2\theta_n + \Delta\theta_i^d + \Delta\theta_o)\right] \\ &+ \frac{V_n(\Delta\omega_o T_n/4)}{2}\left[-\sin(\Delta\theta_i - \Delta\theta_o) + \sin(2\theta_n + \Delta\theta_i + \Delta\theta_o)\right] \quad (6) \end{aligned}$$

$$\begin{aligned} v_q(t) &\approx \frac{V_n + \Delta V_i}{2}\left[\sin(\Delta\theta_i - \Delta\theta_o) - \sin(2\theta_n + \Delta\theta_i + \Delta\theta_o)\right] \\ &+ \frac{V_n + \Delta V_i^d}{2}\left[\sin(\Delta\theta_i^d - \Delta\theta_o) + \sin(2\theta_n + \Delta\theta_i^d + \Delta\theta_o)\right] \\ &+ \frac{V_n(\Delta\omega_o T_n/4)}{2}\left[\cos(\Delta\theta_i - \Delta\theta_o) + \cos(2\theta_n + \Delta\theta_i + \Delta\theta_o)\right] \quad (7) \end{aligned}$$

By assuming that $\Delta\theta_i \approx \Delta\theta_o$ and $\Delta V_i \approx \Delta V_o$, (6) and (7) can be linearized as

$$\begin{aligned} v_d(t) &\approx V_n + \frac{1}{2}(\Delta V_i + \Delta V_i^d) + \frac{\cos(2\theta_n)}{2}(\Delta V_i - \Delta V_i^d) \\ &- \frac{V_n \sin(2\theta_n)}{2}(\Delta\theta_i - \Delta\theta_i^d - \Delta\omega_o T_n/4) \quad (8) \end{aligned}$$

$$\begin{aligned} v_q(t) &\approx \frac{V_n}{2}(\Delta\theta_i + \Delta\theta_i^d) - V_n\Delta\theta_o + \frac{V_n}{2}\Delta\omega_o T_n/4 \\ &- \frac{V_n \cos(2\theta_n)}{2}(\Delta\theta_i - \Delta\theta_i^d - \Delta\omega_o T_n/4) \\ &- \frac{\sin(2\theta_n)}{2}(\Delta V_i - \Delta V_i^d). \quad (9) \end{aligned}$$

Using (8) and (9), the LTP model of the ATD-PLL can be obtained as depicted in Fig. 4(a).

In this stage, it may be interesting to see what is the difference between the derived LTP model for the ATD-PLL and the existing LTI one. The only input to the LTI model of the ATD-PLL [9], as shown in Fig. 4(b), is the phase perturbation $\Delta\theta_i$, because the input signal amplitude variations have been neglected in obtaining this model [9]. The LTP model, however, receives both the phase and amplitude
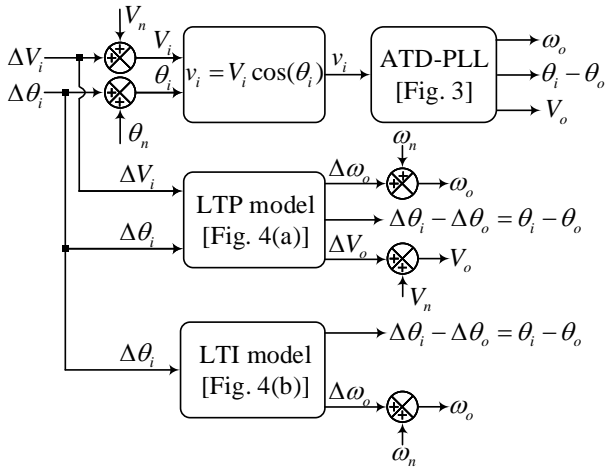
Fig. 5. Schematic diagram of the procedure for the numerical model verification.

perturbations as its input signals. It implies that the LTI model, contrary to the LTP one, may not be able to predict transient states of the ATD-PLL in response to an amplitude change (e.g., a voltage sag or swell) in its input. Besides, the coupling between the upper and lower parts of the LTP model implies that the phase and amplitude parameters in the ATD-PLL are dynamically coupled. The existing LTI model may not be able to predict this coupling.

B. Numerical Model Verification

This section aims to test the accuracy of the derived LTP model for the ATD-PLL in comparison with the LTI one. To this end, some small perturbations in the phase, frequency, and amplitude of the single-phase input signal of the ATD-PLL are programmed first. The same perturbations are applied to the LTP and LTI models of the ATD-PLL. The ATD-PLL outputs are finally compared with the prediction of its models. Fig. 5 illustrates this procedure. The control parameters k_p and k_i of the ATD-PLL are selected the same as those chosen in [9], i.e., $k_p = 217$ and $k_i = 15791$. The cutoff frequency ω_v is set to $2\pi 25$ rad/s. The nominal amplitude and frequency of the input signal and the sampling frequency are considered as 1 p.u., 50 Hz, and 8 kHz, respectively.

Figs. 6-8 show the evaluation results. From these plots, the following observations can be made.

- The LTI model cannot predict transient states in the ATD-PLL output amplitude regardless of the cause of this transient, which can be a change in the frequency, phase, or amplitude [see bottom plots in Figs. 6, 7, and 8].
- The LTI model cannot predict transient states in the output phase and frequency when a change in the input signal amplitude happens [see Fig. 8].
- The LTI model cannot predict the damped double-frequency oscillations that exist in the ATD-PLL transient behavior. This inaccuracy will be more noticeable if the ATD-PLL bandwidth is increased.
- The LTP model does not have the above limitations of the LTI one and, therefore, provides much higher accuracy in predicting the dynamics of the ATD-PLL.
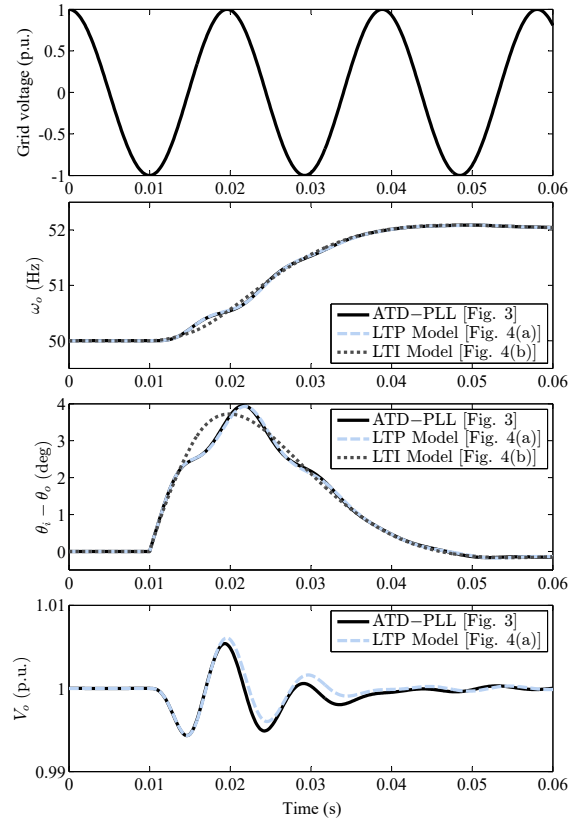

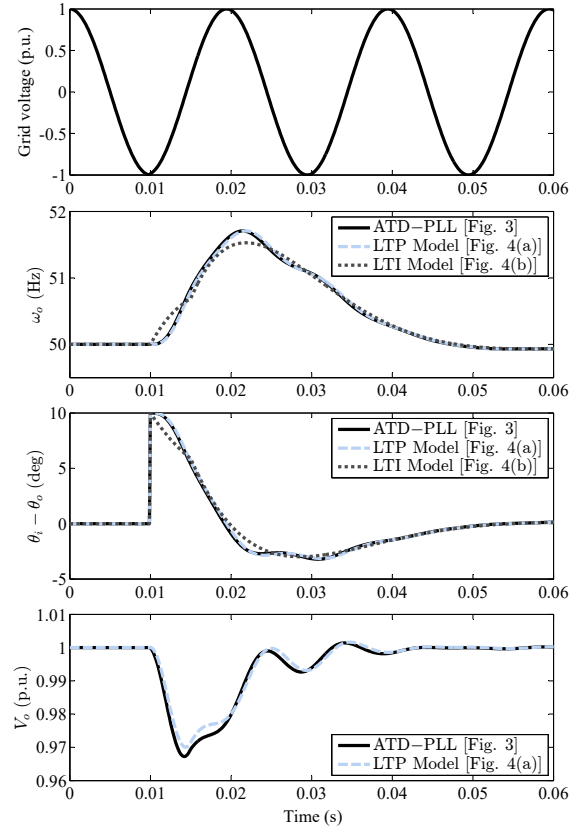Fig. 6. Numerical model verification in response to +2 Hz frequency jump.

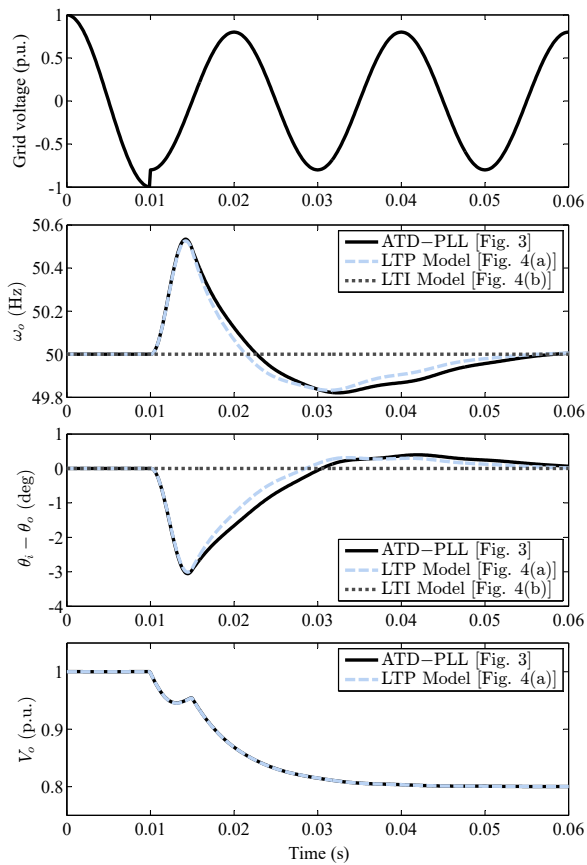Fig. 7. Numerical model verification in response to 10° phase jump.

Fig. 8. Numerical model verification in response to 0.2 p.u. voltage sag.

C. Stability Analysis

The dashed box in Fig. 4(a) is the concerned feedback loop for the stability analysis of the ATD-PLL. The signal $\Delta\omega_o$ in this box, however, is multiplied by a cosine term, which makes the concept of transfer function elusive here. To deal with this challenge, one can simply replace the cosine term by its equivalent expression in terms of exponentials, i.e., $\cos(2\theta_n) = \cos(2\omega_n t) = \frac{e^{j2\omega_n t} + e^{-j2\omega_n t}}{2}$, and obtain

$$
\begin{aligned}
\Delta\theta_e(s) = &-\frac{T_n k_i (s - j2\omega_n)/16}{k_p(s - j2\omega_n) + k_i}\Delta\theta_o(s - j2\omega_n) \\
&+ \frac{s(s - V_n T_n k_i/8)}{V_n(k_p s + k_i)}\Delta\theta_o(s) \\
&- \frac{T_n k_i(s + j2\omega_n)/16}{k_p(s + j2\omega_n) + k_i}\Delta\theta_o(s + j2\omega_n).
\end{aligned}
\tag{10}
$$

By substituting the Laplace operator s by $s + j2m\omega_n$ in (10), where $m \in \mathbb{Z}$, one can achieve

$$
\begin{aligned}
\Delta\theta_e&(s + j2m\omega_n) = \\
&-\frac{T_n k_i(s + j2(m-1)\omega_n)/16}{k_p(s + j2(m-1)\omega_n) + k_i}\Delta\theta_o(s + j2(m-1)\omega_n) \\
&+\frac{(s + j2m\omega_n)((s + j2m\omega_n) - V_n T_n k_i/8)}{V_n(k_p(s + j2m\omega_n) + k_i)}\Delta\theta_o(s + j2m\omega_n) \\
&-\frac{T_n k_i(s + j2(m+1)\omega_n)/16}{k_p(s + j2(m+1)\omega_n) + k_i}\Delta\theta_o(s + j2(m+1)\omega_n)
\end{aligned}
\tag{11}
$$

which is corresponding in the matrix form to (12) at the top of the next page. This doubly infinite matrix equation, which relates the frequency components of $\Delta\theta_o$ to $\Delta\theta_e$, is the inverse of the open-loop harmonic transfer function (HTF) of the ATD-PLL. By considering a truncated version of (12) and obtaining its eigenloci, one can evaluate the stability of the ATD-PLL and determine its stability margins [13]–[15].

Here, it can be interesting to see the difference between the LTI and LTP models of the ATD-PLL in assessing its stability. From the LTI model of the ATD-PLL in Fig. 4(b), the closed-loop transfer function can be obtained as [9]

$$
\begin{aligned}
G_{cl}^{LTI} &= \frac{\Delta\theta_o(s)}{\Delta\theta_i(s)} \\
&= \frac{1 + e^{-\frac{T_n s}{4}}}{2} \frac{V_n(k_p s + k_i)}{s^2 + V_n(k_p - k_i T_n/8)s + V_n k_i}.
\end{aligned}
\tag{13}
$$

By applying the Routh–Hurwitz stability criterion to (13), it can be found that the LTI stability of the ATD-PLL requires $0 < k_i < \frac{8}{T_n}k_p$ or equivalently $0 < k_i < 400 k_p$. The solid lines in Fig. 9, which show the LTI phase margin (PM) of the ATD-PLL as a function of k_i, help to better visualize this fact. Notice that in the upper, middle, and lower plots of this figure, which are corresponding to $k_p = 200$, 250, and 300, respectively, the LTI PM becomes zero when k_i reaches $8e4$, $10e4$, and $12e4$, respectively. The LTP model, however, shows that the stability margin of the ATD-PLL and the stability range of its control parameters are actually more limited than what its LTI model is predicting (see dashed lines in Fig. 9). This is particularly true when the control gains k_p and k_i are large. Notice that the stability predictions of the LTP model can be easily verified numerically. Here, to save space, the numerical versification is not presented.

D. Modeling Extension to Other TD-PLLs

The LTP modeling of other $T/4$ delay-based PLLs can be carried out by following a similar procedure as presented in section II-A for the ATD-PLL. In some cases, however, this mathematical procedure may be avoided. For instance, the basic TD-PLL in Fig. 1 is corresponding to remove the frequency feedback loop in the ATD-PLL structure in Fig. 3. Therefore, the LTP model of the basic TD-PLL may be obtained by removing all feedback loops connected to the signal $\Delta\omega_o$ in Fig. 4(a). The resulting LTP model is shown in Fig. 10. As another example, consider the VLTD-PLL in Fig. 2. It has been proven in [10] that the VLTD-PLL is mathematically equivalent to the ATD-PLL. Therefore, both of them have the same LTP model.

E. Limitations

The LTP model derived for the ATD-PLL has two limitations, which need to be briefly discussed here. The first limitation is that the accuracy of the LTP model drops with increasing the magnitude of the input disturbance. Comparing Fig. 11, which shows the model verification results in response to a large voltage sag (0.5-p.u. voltage sag), with those in Fig. 8 confirms this fact. The reason behind this limitation is that
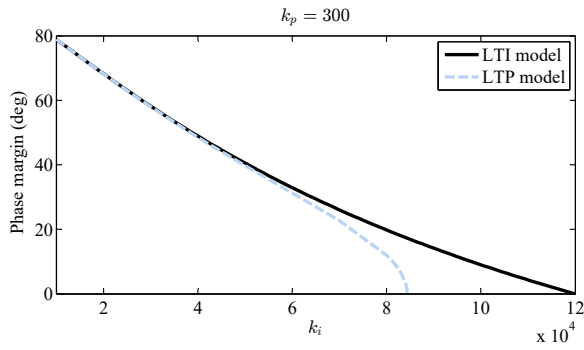
$$
\begin{pmatrix}
\vdots \\
\Delta\theta_e(s-j2\omega_n) \\
\Delta\theta_e(s) \\
\Delta\theta_e(s+j2\omega_n) \\
\vdots
\end{pmatrix}
=
\underbrace{
\begin{pmatrix}
\ddots & \vdots & \vdots & \vdots & \cdot^{\cdot^{\cdot}} \\
\cdots & \frac{(s-j2\omega_n)((s-j2\omega_n)-V_nT_nk_i/8)}{V_n(k_p(s-j2\omega_n)+k_i)} & -\frac{T_nk_is/16}{k_ps+k_i} & 0 & \cdots \\
\cdots & -\frac{T_nk_i(s-j2\omega_n)/16}{k_p(s-j2\omega_n)+k_i} & \frac{s(s-V_nT_nk_i/8)}{V_n(k_ps+k_i)} & -\frac{T_nk_i(s+j2\omega_n)/16}{k_p(s+j2\omega_n)+k_i} & \cdots \\
\cdots & 0 & -\frac{T_nk_is/16}{k_ps+k_i} & \frac{(s+j2\omega_n)((s+j2\omega_n)-V_nT_nk_i/8)}{V_n(k_p(s+j2\omega_n)+k_i)} & \cdots \\
\cdot^{\cdot^{\cdot}} & \vdots & \vdots & \vdots & \ddots
\end{pmatrix}
}_{\mathcal{HTF}_i(s)}
\begin{pmatrix}
\vdots \\
\Delta\theta_o(s-j2\omega_n) \\
\Delta\theta_o(s) \\
\Delta\theta_o(s+j2\omega_n) \\
\vdots
\end{pmatrix}
$$

$$(12)$$
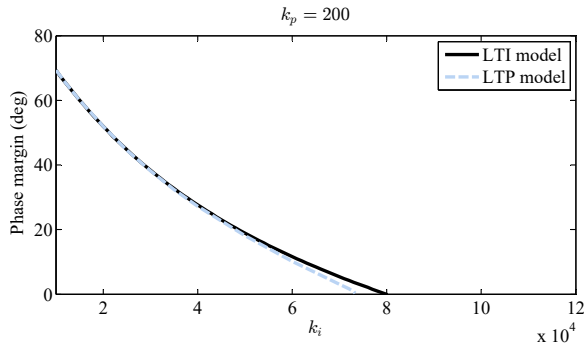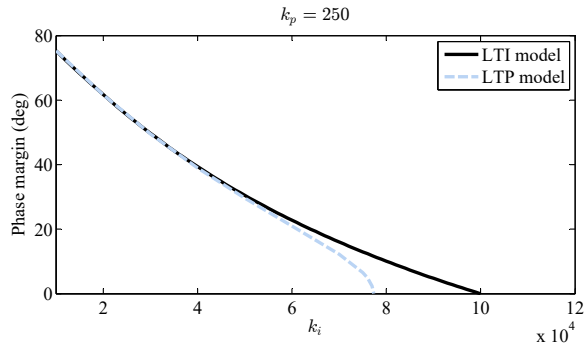
Fig. 9. Determining the PM of the ATD-PLL as a function of k_i using its LTI and LTP models. (a) $k_p = 200$. (b) $k_p = 250$. (c) $k_p = 300$.

the LTP model is obtained by assuming small-signal perturbations around a periodic trajectory. A large-signal disturbance
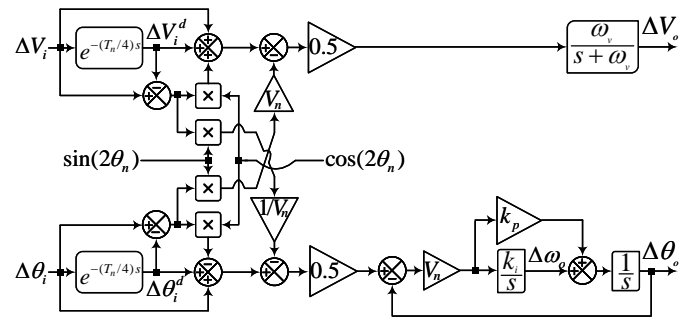

Fig. 10. LTP model of the basic TD-PLL.

is not consistent with this assumption and, therefore, results in a reduced accuracy.

The second limitation is that the derived LTP model for the ATD-PLL neglects the presence of harmonic components, which often exist in the grid voltage. Notice that these harmonics result in some oscillatory ripples in the output of the ATD-PLL, but the LTP model is not able to predict them. This fact can be clearly observed in Fig. 12.

III. CONCLUSIONS

The primary aim of this letter was the LTP modeling of $T/4$ delay-based PLLs. To this end, the ATD-PLL was considered as the case study. Thorough a mathematical procedure, an LTP model for the ATD-PLL was obtained, and its accuracy was evaluated through some numerical tests. To highlight the high accuracy of the obtained LTP model, the predicted results from the LTI model of the ATD-PLL were also shown and considered as a reference for the comparison. The stability assessment of the ATD-PLL using its LTP and LTI models were also presented and compared. Finally, the limitations of the derived LTP model and expending it to other TD-PLLs were briefly discussed.

REFERENCES

[1] S. Golestan, J. M. Guerrero, and J. C. Vasquez, "Single-phase PLLs: A review of recent advances," *IEEE Trans. Power Electron.*, vol. 32, no. 12, pp. 9013–9030, Dec. 2017.

[2] M. Karimi-Ghartemani, "A unifying approach to single-phase synchronous reference frame PLLs," *IEEE Trans. Power Electron.*, vol. 28, no. 10, pp. 4550–4556, Oct. 2013.
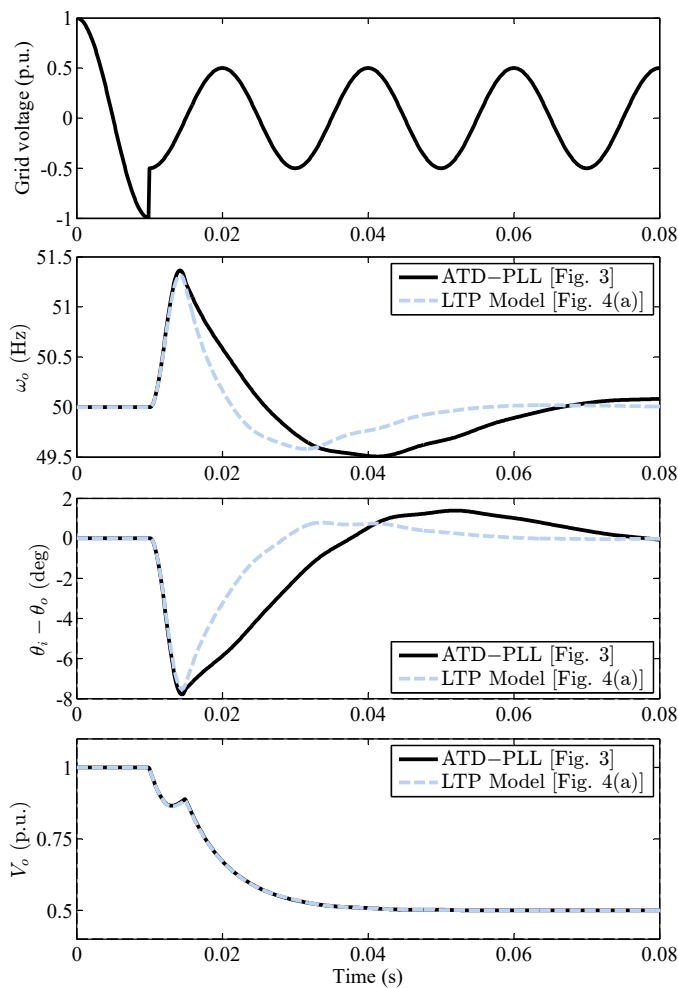
Fig. 11. Numerical model verification in response to 0.5 p.u. voltage sag.
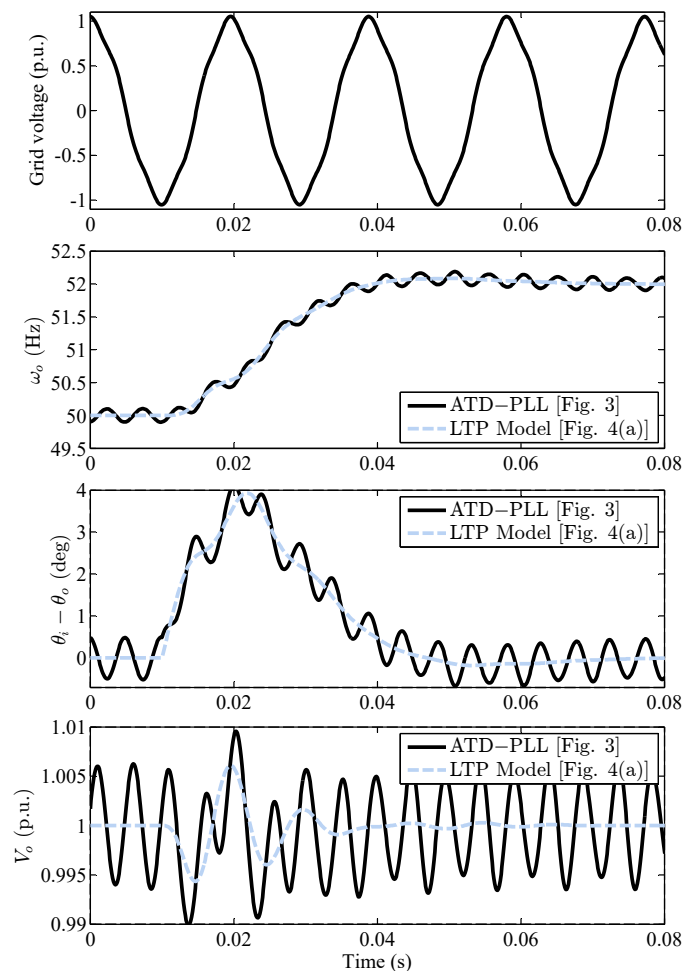

Fig. 12. Numerical model verification in the presence of 0.05-p.u. fifth harmonic and 2-Hz frequency jump in the grid voltage.

[3] M. Ciobotaru, R. Teodorescu, and F. Blaabjerg, "A new single-phase PLL structure based on second order generalized integrator," in *Proc. 37th IEEE Power Electron. Spec. Conf., 2006*, Jun. 2006, pp. 1–6.

[4] S. Golestan, J. M. Guerrero, J. C. Vasquez, A. M. Abusorrah, and Y. A. Al-Turki, "All-pass-filter-based PLL systems: Linear modeling, analysis, and comparative evaluation," *IEEE Trans. Power Electron.*, vol. 35, no. 4, pp. 3558–3572, Apr. 2020.

[5] R. M. S. Filho, P. F. Seixas, P. C. Cortizo, L. A. B. Torres, and A. F. Souza, "Comparison of three single-phase PLL algorithms for UPS applications," *IEEE Trans. Ind. Electron.*, vol. 55, no. 8, pp. 2923–2932, Aug. 2008.

[6] S. Foyen, C. Zhang, O. Fosso, and M. Molinas, "Frequency domain modelling for assessment of Hilbert and SOGI based single-phase synchronisation," in *Proc. IEEE IECON*, vol. 1, 2019, pp. 1780–1785.

[7] K. De Brabandere, T. Loix, K. Engelen, B. Bolsens, J. Van den Keybus, J. Driesen, and R. Belmans, "Design and operation of a phase-locked loop with Kalman estimator-based filter for single-phase applications," in *Proc. IEEE IECON*, 2006, pp. 525–530.

[8] C. Subramanian and R. Kanagaraj, "Single-phase grid voltage attributes tracking for the control of grid power converters," *IEEE J. Emerg. Sel. Topics Power Electron.*, vol. 2, no. 4, pp. 1041–1048, Dec. 2014.

[9] S. Golestan, J. M. Guerrero, A. Abusorrah, M. M. Al-Hindawi, and Y. Al-Turki, "An adaptive quadrature signal generation-based single-phase phase-locked loop for grid-connected applications," *IEEE Trans. Ind. Electron.*, vol. 64, no. 4, pp. 2848–2854, Apr. 2017.

[10] S. Golestan, J. M. Guerrero, J. C. Vasquez, A. M. Abusorrah, and Y. Al-Turki, "Research on variable-length transfer delay and delayed-signal-cancellation-based PLLs," *IEEE Trans. Power Electron.*, vol. 33, no. 10, pp. 8388–8398, Oct. 2018.

[11] S. Golestan, J. M. Guerrero, A. Vidal, A. G. Yepes, J. Doval-Gandoy, and F. D. Freijedo, "Small-signal modeling, stability analysis and design

optimization of single-phase delay-based PLLs," *IEEE Trans. Power Electron.*, vol. 31, no. 5, pp. 3517–3527, May. 2016.

[12] Y. Yang, K. Zhou, and F. Blaabjerg, "Exploitation of digital filters to advance the single-phase T/4 delay PLL system," in *Proc. IEEE South. Power Electron. Conf. (SPEC)*, Dec. 2016, pp. 1–6.

[13] S. R. Hall and N. M. Wereley, "Generalized nyquist stability criterion for linear time periodic systems," in *1990 American Control Conference*, May. 1990, pp. 1518–1525.

[14] M. Pachter, T. Kobylarz, and C. Houpis, "Literal nyquist stability criterion for MIMO control systems," *Int. J. Control*, vol. 63, no. 1, pp. 55–65, 1996.

[15] S. Golestan, J. M. Guerrero, J. C. Vasquez, A. M. Abusorrah, and Y. A. Al-Turki, "Standard SOGI-FLL and its close variants: Precise modeling in LTP framework and determining stability region/robustness metrics," *IEEE Trans. Power Electron.*, vol. PP, no. 99, pp. 1–12, May. 2020.